Available online at www.sciencedirect.com
SCIENCE DIRECT®
Journal of the European Ceramic Society 25 (2005) 719–728
www.elsevier.com/locate/jeurceramsoc

Development of a morphological texture in relation with the crystallographic texture during sintering of strontium hexaferrites

C. Genevois [a], J.-M. Missiaen [a,*], F. Robaut [b], F. Grillon [c], C. P. Carry [a]

[a] *INPG, Laboratoire de Thermodynamique et de Physico-Chimie Métallurgiques (UMR 5614, CNRS-INPG/UJF), Domaine Universitaire, BP 75, 38402 Saint-Martin d'Hères, France*
[b] *INPG, Consortium des Moyens Technologiques Communs, Domaine Universitaire, BP 75, 38402 Saint-Martin d'Hères, France*
[c] *E.N.S. des Mines, Centre des Matériaux P.M. Fourt (UMR 7633, CNRS), BP 87, 91003 Evry Cedex, France*

Received 12 September 2003; received in revised form 5 April 2004; accepted 20 April 2004

Available online 26 June 2004

Abstract

Quantitative analysis of grain size, grain shape, morphological and crystallographic texture has been performed in strontium hexaferrites materials, sintered from filter-pressed powders oriented or not with a magnetic field. The results provide evidence for anisotropic and abnormal grain growth at high temperature ($T \geq 1250\,^{\circ}C$). A morphological texture develops during heating for oriented samples, with plate-like grains preferentially aligned with their larger facets perpendicular to the direction of field application. A quantitative analysis of the morphological texture in 3D has been performed and the relation between morphological and crystallographic texture is identified from the results. The increase in crystallographic texture is related to grain growth.

Keywords: Ferrite; Grain growth; Hard magnets; Sintering; Texture

1. Introduction

Introducing a crystallographic texture in polycrystalline ceramics is a way to combine anisotropic properties of a single-crystal with the beneficial properties and the easier shape-forming of a polycrystalline material. In ferroelectric or ferromagnetic materials, the saturation polarization or magnetization may reach values close to those of the single-crystal in the direction of anisotropy, together with a high remanent polarization or magnetization.[1–4] The critical current in superconducting materials may also be increased by suitable texture.[5–8] In structural ceramics, texturing produces anisotropic elastic properties and may significantly change the crack path during fracture.[9]

Powder processes to create a crystallographic texture generally involve orienting anisotropically shaped particles. For materials with anisotropic hexagonal or tetragonal structures, powders may exhibit plate-like morphologies, due to the anisotropy in surface or interface energy, the shape of platelets being related to the crystallographic orientation of the crystals. Crystallographic texture can then be obtained by orienting the platelets through tape casting,[10] uniaxial pressing,[11,12] vibration,[8] powder injection molding,[3] hot pressing or hot forging.[7,13–15] A better control of the texture after forming may be obtained by the templated grain growth process (TGG). In this process, large anisotropically shaped particles are used as templates for grain growth and are oriented in a fine-particle-size matrix by tape casting or uniaxial pressing.[4,16–19] The crystallographic texture in such cases is closely bound to a morphological texture, since it originates from a preferential alignment of plate-like grains in the green body.

An alternative for creating a crystallographic texture in the case of hard ferromagnetic materials is to orient particles under a magnetic field. NdFeB or hexagonal ferrite particles tend to align with their c crystallographic axis parallel to the magnetic field, due to the strong magnetocrystalline anisotropy of these structures.[20,21] In that case, a strong crystallographic texture may be created even with equiaxed particles and the crystallographic texture is much stronger than the morphological texture.

The crystallographic and morphological texture may vary during sintering. During hot-forged or hot-pressed

* Corresponding author. Tel.: +33 4768 26676; fax: +33 4768 26744.
E-mail address: missiaen@ltcpm.inpg.fr (J.-M. Missiaen).

0955-2219/$ – see front matter © 2004 Elsevier Ltd. All rights reserved.
doi:10.1016/j.jeurceramsoc.2004.04.012

experiments, grain rotation via grain boundary sliding usually enhances the texture.[14,15] In free sintering experiments, grain rotation via rearrangement may disturb the initial texture but this effect is usually considered to be negligible.[18,21] Variation of the morphological texture in that case is attributed to anisotropic grain growth.[1,4,9,11,16,18,19,21–23] Quantitative analysis of the correlation between variations of the morphological and of the crystallographic texture has only been performed in the case of templated grain growth[9,16,18,19,22] or of composites with dispersed very large platelets in a fine-matrix secondary phase.[24] In such cases, the volume of crystallographically textured material equals the volume of large platelets and the distribution of crystallographic and morphological orientations are similar.[18,19,24] The situation is not so simple when starting with powders with a more uniform microstructure, when oriented particles have not necessary a size advantage for grain growth, and when the particle shapes are not strongly correlated to the crystallographic orientations. The aim of this work is to analyse the development of a morphological texture in relation with the crystallographic texture during the sintering of strontium hexaferrites, where particles are oriented under a magnetic field and the initial crystallographic texture is more pronounced than the morphological texture.

2. Experimental procedure

2.1. Samples preparation

Strontium hexaferrite $SrFe_{12}O_{19}$ powders were filter-pressed with a disc shape up to a green density around 50%, either under a magnetic field oriented parallel to the compaction axis, or without magnetic field. The compaction and magnetic field direction constitute an anisotropy axis *Z* for the sample (Fig. 1). The magnetic field induces a crystallographic [0 0 0 1] fiber texture in the green compacts, due to the strong magnetocrystalline anisotropy of the structure. Cubic samples were cut out of these discs and heated under air at 1 °C/min up to 1250 or 1300 °C. Samples prepared under a magnetic field will be referred to as “oriented samples” in the following.

The sintered specimen were cut parallel to the anisotropy axis and mechanically polished down to 1/4 μm. They were then annealed for two hours at 1080 °C in order to relax polishing induced damage and to etch grain boundaries.

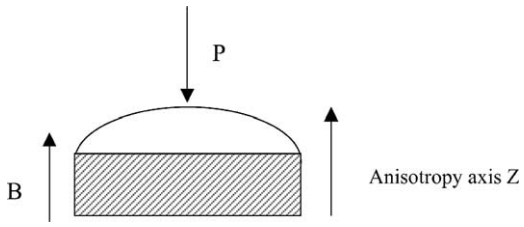

Fig. 1. Schematic representation of filter-pressing under a magnetic field, and representation of the anisotropy axis.

2.2. EBSD analysis

The local crystallographic texture was analysed with a scanning electron microscope (SEM) via electron backscattering diffraction (EBSD) using the orientation imaging microscopy (OIM) software of TechSEM Laboratories (TSL). Pole figures are currently obtained by this technique. In order to quantify the fiber texture in our case, the distribution of orientations of the [0 0 0 1] axis relatively to the anisotropy axis was also computed for all the points analysed. Point fractions in each class of orientation were divided by the total solid angle in the class, so that fractions/unit solid angle in different classes can be directly compared. From a stereological point of view, these point fractions are estimates of the volume fractions of ferrite phase in each class of orientation. Local texture information was also correlated to local morphological information obtained by image analysis (see the following).

Samples sintered at 1300 °C had a grain size in the range 10–100 μm and could be analysed with a conventional SEM equipped with a tungsten thermionic gun (JEOL 840A). The main Kikuchi lines were first calculated with the software by inputting the atomic positions of the complex $SrFe_{12}O_{19}$ hexagonal structure. The oriented sample was introduced into the chamber with the anisotropy axis parallel to the tilt axis of the EBSD device. In these conditions, the sharpest (0 0 0 2) reflection yields a vertical line on the diagram for a perfectly oriented grain. Parameters of the Hough transform which is used to index the Kikuchi diagrams were optimised in this case. Orientation maps could then be automatically obtained (Fig. 2a) and the distribution of orientations computed. 500 to 1000 grains/sample were analysed in this way.

Samples sintered at 1250 °C had a grain size around 1 μm, and had to be analysed with a SEM equipped with a field emission gun (GEMINI ZEISS DSM 982). The orientation of the sample, the reflection lines and the Hough parameters were those already used in the analysis of the large grain samples. Nevertheless, automatic mapping could not be realised in that case due to the lack of resolution, and to the surface topography which induced shading zones on the diagrams. Consequently, the texture was analysed by a manual pointing of the best zone in each grain, and a semi-automatic indexation of the Kikuchi diagrams. Orientation maps could then be plotted a posteriori by labelling the SEM deduced binary image of the grains (Fig. 3). Pole figures and distribution of orientations were computed as before. About 200 grains only were analysed by this technique for the oriented sample.

2.3. Image analysis

The grain morphology and orientation were quantified by analysis of SEM or EBSD images after various image processings.

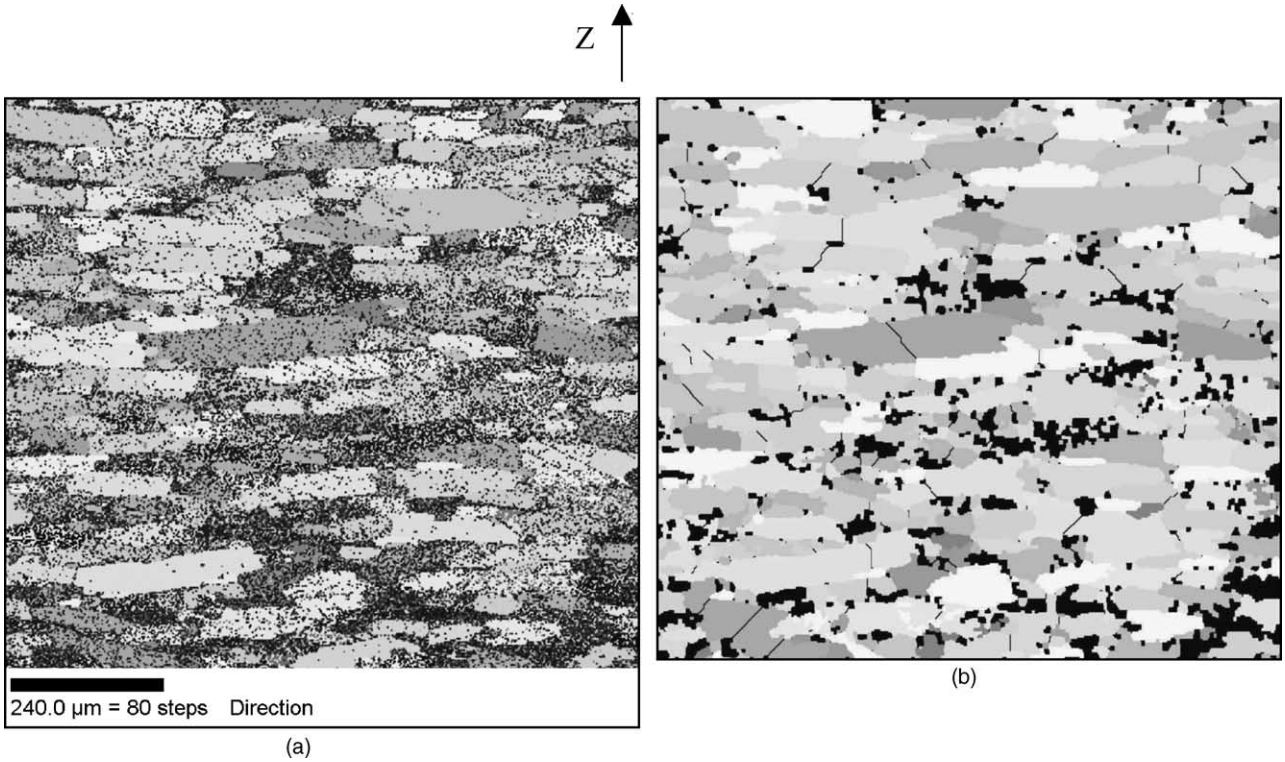

Fig. 2. (a) Crystallographic orientation map of the oriented sample sintered at 1300 °C, obtained by EBSD automatic mapping. (b) Image of crystallographic grains after treatment. (The grey level code uses a linear function of the misorientation of the [0 0 0 1] axis and the anisotropy axis *Z*; black pixels represent pores or pixels that could not be affected to grains.)

For the 1250 °C sintered sample, the morphology and orientation of the grains was quantitatively analysed by using SEM images in the secondary electron mode (Fig. 4a). An edge detection was performed with a Sobel filter to enhance contrast on grain boundaries and a binary image of the grains was obtained after thresholding (Fig. 4b). Several thousands of grains/sample were analysed in this way.

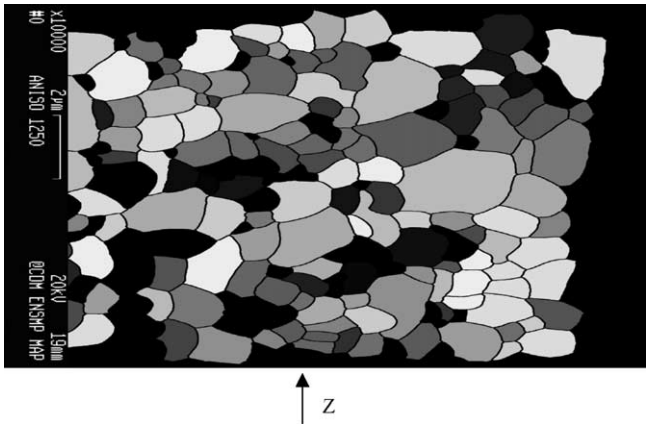

Fig. 3. Crystallographic orientation map of the oriented sample sintered at 1250 °C, reconstructed from binary images deduced from SEM and labelled using results of manual EBSD pointing. (The grey level code uses a linear function of the misorientation of the [0 0 0 1] axis and the anisotropy axis *Z*; black pixels represent pores or pixels that could not be affected to grains.)

For the 1300 °C sintered sample, crystallographic orientation maps obtained by EBSD (Fig. 2a) were processed. Images were smoothed using crystallographic orientation criteria of the neighbouring points with the OIM software. The final images contained information concerning both the microstructure and the crystal orientations (Fig. 2b).

In both cases, images were cleaned by using standard morphological filters, a final separation of the grains was performed with an automatic segmentation algorithm (Figs. 2b and 4b), and measurements were performed with the APHELION software (ADCIS S.A & Amerinex Applied Imaging, Inc.).

Quantitative analysis of the grain morphology was performed. The 2D equivalent grain size distribution and average shape factor of the grains was determined. The 2D equivalent diameter is defined as the diameter of the disc having the same area as that of the grain. The 2D shape factor is defined as the ratio of the length to the width of the smallest rectangle containing the grain.

Morphological orientation of the grains was quantified too by computing different orientation indexes, defined as the ratios of average sizes measured in the direction perpendicular (⊥) and parallel (||) to the *Z*-axis. The morphological orientation indexes which were used are:

- $L_{\perp}/l_{||}$: ratio of the average projections of the grains
- $L_{1g_{\perp}}/l_{1g_{||}}$: ratio of the average mean intercept lengths of the grains

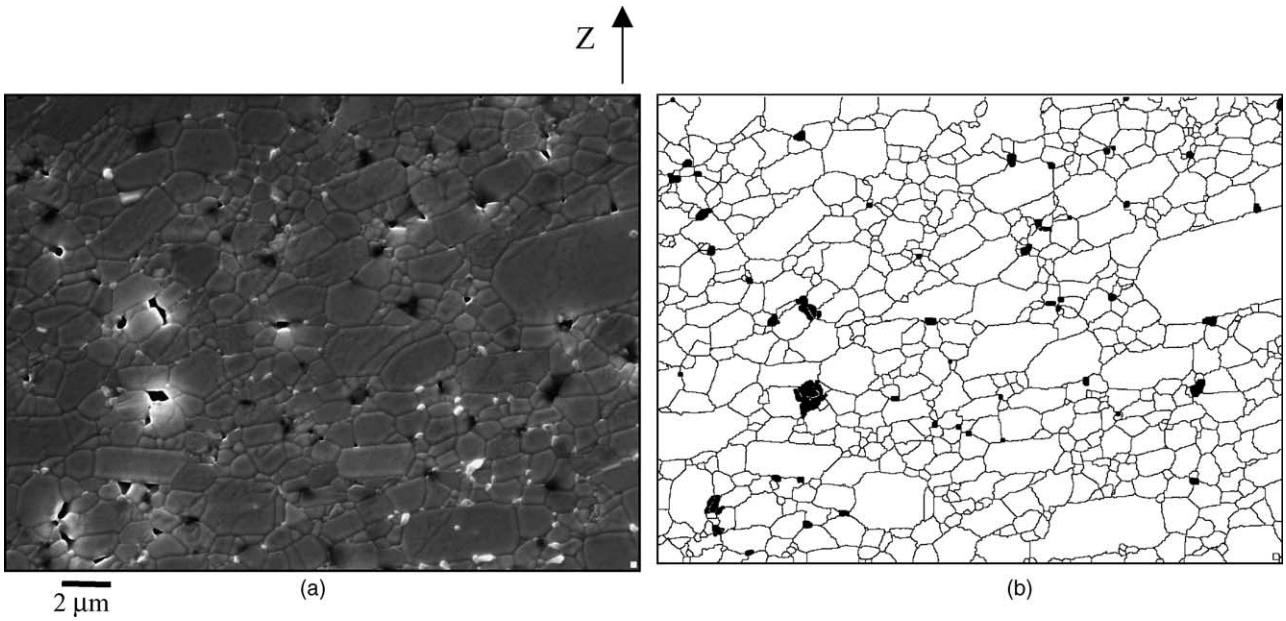

Fig. 4. (a) SEM image of the oriented sample sintered at 1250 °C (polished section). (b) Binary image after treatment.

- $L_{1_\perp}/l_{1_\parallel}$: ratio of the average intercept lengths of the phase (i.e. the average intercept length is computed on the whole set of grains)

The orientation of the grains was also quantified with a shape-orientation diagram, representing the shape factor, i.e. the ratio of the length to the width of the smallest rectangle containing the grain, as a function of the misorientation of the rectangle with respect to the anisotropy axis (Fig. 5).

2.4. Reconstruction of the 3D morphological texture

Distribution of orientations of the smallest rectangles containing the grains can be assumed to represent the distribution of the 2D cross-section normals to the plate-like grains (Fig. 5). Reconstruction of the 3D orientation distribution was performed following a similar approach to that used in reference.[24]

Let us consider a 2D grain section in a plane containing the anisotropy axis *Z*, having its cross-section normal oriented between θ and $\theta + d\theta$ with respect to *Z*. The 3D normal orientation can describe a circular band, depending on the angle ϕ between the 2D and 3D normals (Fig. 6). The volume fraction of such grains is given by:

$$f(\theta)\,d\theta = \int_0^{\pi/2} P(\omega(\theta,\phi))\cos\phi\,d\theta\,d\phi \quad (1)$$

where $\omega(\theta, \phi)$ is the angular misorientation between the 3D-normal and the anisotropy axis and $P(\omega)$ is the volume fraction of grains/unit solid angle oriented at ω with respect to the anisotropy axis. This angle can be related to θ and ϕ from simple geometrical considerations:

$$\omega(\theta,\phi) = a\cos(\cos\theta\cos\phi) \quad (2)$$

There is no general solution to the problem of reconstruction of the 3D orientation distribution $P(\omega)$ from the measured 2D distribution $f(\theta)$. Here it is assumed that the 3D distribution is axisymmetric and that it can be modelled by the

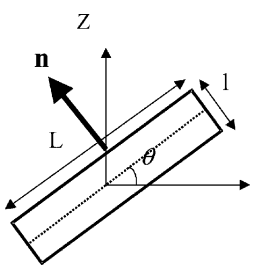

Fig. 5. 2D morphological misorientation angle θ.

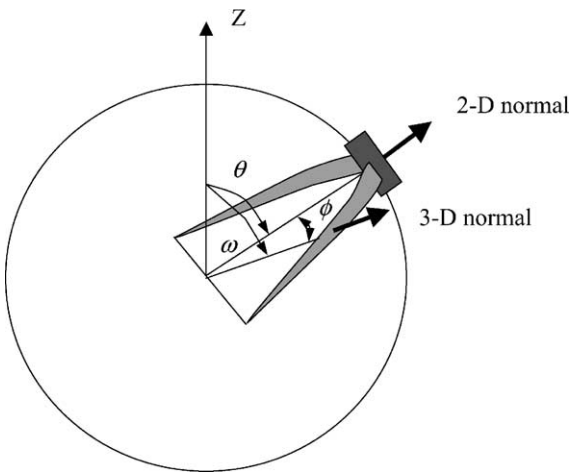

Fig. 6. Relative position of the 2D and 3D normals to plate-like grains.

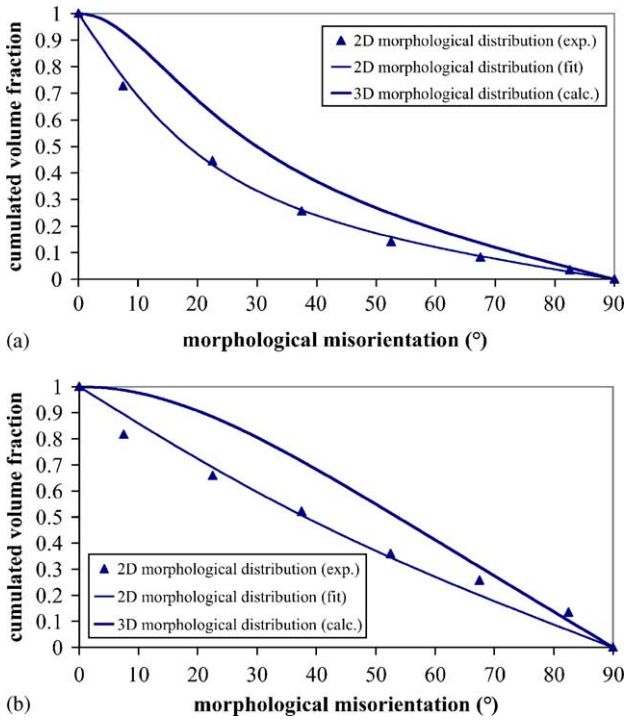

Fig. 7. 2D measured and 3D calculated morphological misorientation for the oriented sample sintered at 1250 °C: (a) oriented sample sintered at 1250 °C, (b) non-oriented sample sintered at 1250 °C.

March–Dollase equation:[22]

$$P(\omega) = \frac{2}{\pi}\left(r^2\cos^2\omega + \frac{1}{r}\sin^2\omega\right)^{-3/2} \quad (3)$$

where r is a factor which quantifies the texture intensity ($r \to 0$ for perfectly aligned grains; $r \to 1$ for a uniform isotropic distribution of orientations). The 3D angular orientation distribution $P(\omega)$ was reconstructed from the 2D measured angular orientation distribution $f(\theta)$ by adjusting parameter r to fit Eq. (1). Fig. 7 gives an example of reconstruction for the oriented and non-oriented samples sintered at 1250 °C.

Some experimental artefacts limit the quality of the reconstruction. At first, the 2D analysis assumes that the 2D cross-section of a grain is elongated in the direction of its 3D largest facets, which is not true for cross-sections which only intersect lateral facets, or which intersect the largest facets but on the edge of the grain (Fig. 8). In this last case, the apparent 2D normal can be associated to the lateral facet cross-sections, i.e. an error around 90° on the 2D orientation. Such events are particularly frequent in the case of poor texture (grains with a shape factor ≈1 and/or isotropic orientation) and will decrease the apparent texture by shifting (about 90°) the orientation of the corresponding profiles. Another source or error may arise from image processing: the digital representation of small and/or nearly isotropic 2D objects can yield errors in the determination of the orientation of the rectangle containing the particle. This error can be important in the case of bad resolution or again in the case of poor texture, but it will tend to redistribute the orientations

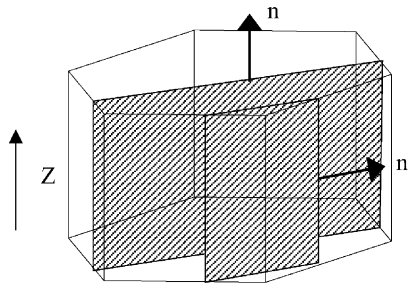

Fig. 8. 2D sections of a grain showing that the direction of the 2D normal may be 90°.

in all directions, creating a background of pseudo-uniform distribution.

Globally, the effect of artefacts is then to redistribute the orientation in all directions and to reinforce the contribution of misorientation around 90° from the anisotropy axis. From a purely empirical point of view, the reconstruction from the whole set of 2D data always underestimates the true 3D texture, particularly in the case of weak texture. In the analysis of templated grain growth, Seabaugh et al.[22] prefer to select those grains with a shape factor higher than 2 before reconstruction to limit the artefacts. This procedure may be valid when the anisotropic grains initially have a high shape factor in 3D but even in that case, the contribution of such grains to small shape factors in 2D is neglected in the reconstruction which induces a bias. In our case where the texture is created from a majority of initially quasi-equiaxed grains, this approach could not be applied. When selecting the grains with the highest 2D shape factors, the texture increased gradually as the critical shape factor was increased until the largest possible value. Therefore we chose to reconstruct the distribution from the whole set of 2D data, which provides an underestimation of the 3D texture.

For the textured sample of Fig. 7a, the distribution background and the weight of misorientations around 90° are rather weak and the artefacts listed above may be neglected. For the non-oriented sample, however, where the texture is weak, this background may be important and the volume fraction oriented in the 80–90° range is abnormally high, due to the artefact explained above (Fig. 7b). The true 2D and 3D texture is then probably more pronounced in that case than predicted from the measurements.

3. Results

3.1. Grain size evolution

Samples sintered at 1250 °C are nearly dense (Table 1). The average grain size increases more than one decade between 1250 and 1300 °C (Table 1). Large grains develop at the expense of the matrix of small micronic grains. At 1300 °C, the large grains fill most of the space but they are still embedded in a matrix of small grains, which were not taken into account in the quantitative analysis (Fig. 2b), due

Table 1
Average microstructural parameters of sintered materials from image analysis measurements

	Sintering temperature (°C)	Porosity	2D average diameter (μm)	2D Shape factor
Oriented	1250	0.015 ± 0.002	0.8 ± 0.1	1.44 ± 0.01
	1300	–	45 ± 2	2.07 ± 0.08
Non-oriented	1250	0.053 ± 0.009	0.9 ± 0.1	1.36 ± 0.01
	1300	–	36 ± 1	1.51 ± 0.01

to the resolution of EBSD images. Anisotropy in grain shape also increases between 1250 and 1300 °C (Table 1). These features are characteristic of abnormal and anisotropic grain growth above 1250 °C.

3.2. Development of a morphological texture

The morphological orientation index is significantly higher than 1 for the oriented samples and it increases sharply between 1250 and 1300 °C (Table 2). This can be interpreted by the development of a morphological texture: plate-like grains which develop due to anisotropic grain growth tend to align with their larger facets perpendicular to the anisotropy axis. Such plate-like grains could indeed be observed on fracture surfaces. The 2D shape-orientation diagrams confirm these results (Fig. 9). A morphological texture is also observed, but much slighter, for non-oriented samples (Table 2).

3.3. Crystallographic texture

Pole figures evidence a marked [0 0 0 1] fiber texture on oriented samples sintered at 1250 °C and 1300 °C, and pratically no texture for the non-oriented sample at 1300 °C (Fig. 10). A quantitative analysis can be performed by comparing the distributions of volume fractions/unit solid angle in each class of orientation (Fig. 11): the crystallographic texture slightly increases between 1250 and 1300 °C for the oriented sample, while a slight but significant texture is also evidenced for the non-oriented sample at 1300 °C.

3.4. Correlation between morphological and crystallographic texture variation

Correlation between crystallographic and morphological texture can be analysed through the comparison of crystallographic orientation distributions (EBSD) and morphological 3D orientation distributions calculated from image analysis data (Figs. 12 and 13).

Table 2
Morphological orientation indexes from image analysis measurements

	Sintering temperature (°C)	$L_{\perp}/l_{\parallel}$	$L_{1g_{\perp}}/l_{1g_{\parallel}}$	$L_{1_{\perp}}/l_{1_{\parallel}}$
Oriented	1250	1.22 ± 0.01	1.18 ± 0.01	1.17 ± 0.01
	1300	1.96 ± 0.07	1.71 ± 0.06	–
Non-oriented	1250	1.08 ± 0.01	1.06 ± 0.01	1.02 ± 0.01
	1300	1.21 ± 0.01	1.17 ± 0.01	–

The increase in crystallographic texture between 1250 and 1300 °C for oriented samples is accompanied by a sharp increase in morphological texture, both distributions becoming much more narrow (Fig. 12). However, the morphological distribution at 1300 °C is still broader than the crystallographic one, with a larger amount of "badly oriented grains", whereas there are practically no grains with a crystallographic misorientation larger than 25°. For non-oriented samples the crystallographic and morphological texture coincide at 1300 °C and the morphological texture hardly evolves between 1250 and 1300 °C (Fig. 13).

3.5. Local correlations between grain size, crystallographic texture, and morphological texture

The advantage of EBSD in the analysis of crystallographic texture is that it provides local information on the crystallographic orientation, which can be correlated

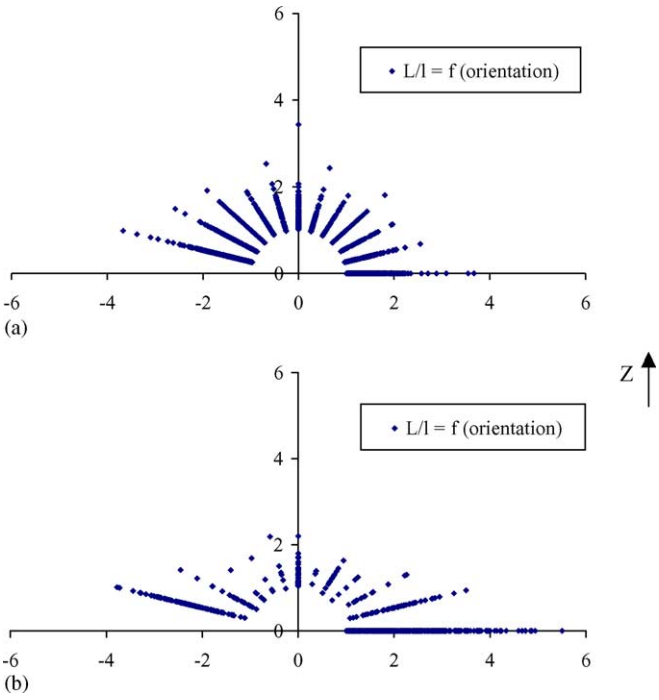

Fig. 9. Representation of the 2D shape factor vs. the orientation: (a) oriented sample sintered at 1250 °C, (b) oriented sample sintered at 1300 °C.

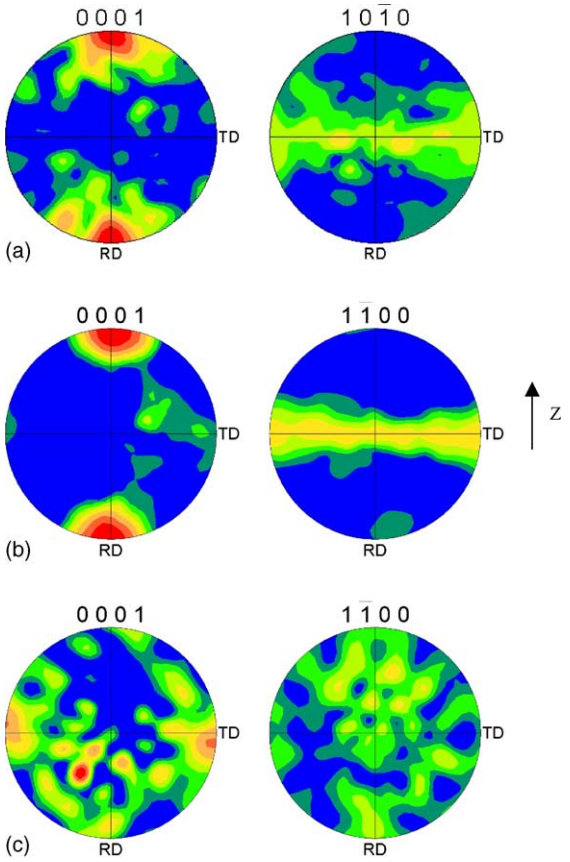

Fig. 10. Pole figures from EBSD analysis: (a) oriented sample sintered at 1250 °C, (b) oriented sample sintered at 1300 °C, (c) non-oriented sample sintered at 1300 °C.

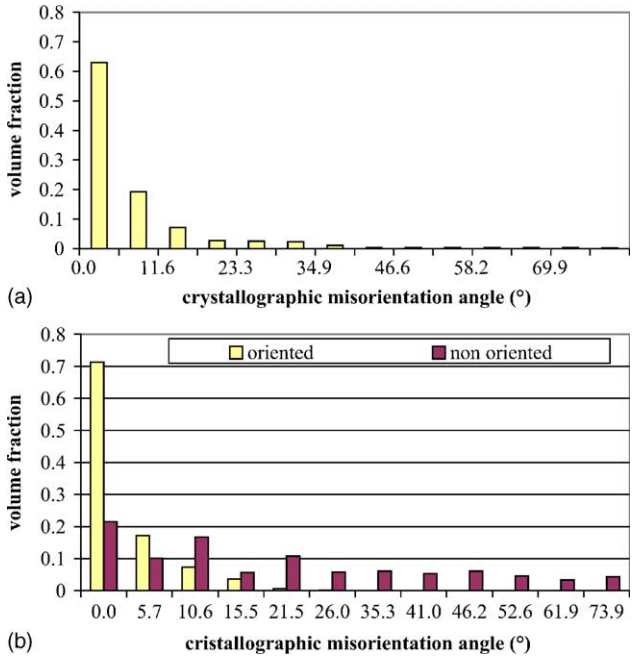

Fig. 11. Distribution of misorientation angles between [0 0 0 1] axis of crystals and the anisotropy axis Z (results are expressed as volume fractions/unit solid angle in each class): (a) oriented sample sintered at 1250 °C, (b) oriented and non-oriented samples sintered at 1300 °C.

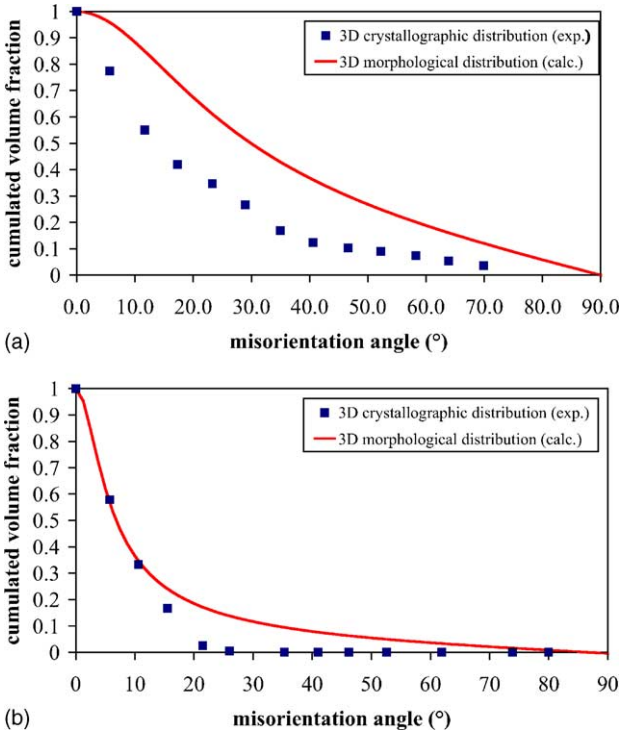

Fig. 12. Cumulated distribution of crystallographic misorientation angles (EBSD measurements) and morphological misorientation angles (from 2D image analyses): (a) oriented sample sintered at 1250 °C, (b) oriented sample sintered at 1300 °C.

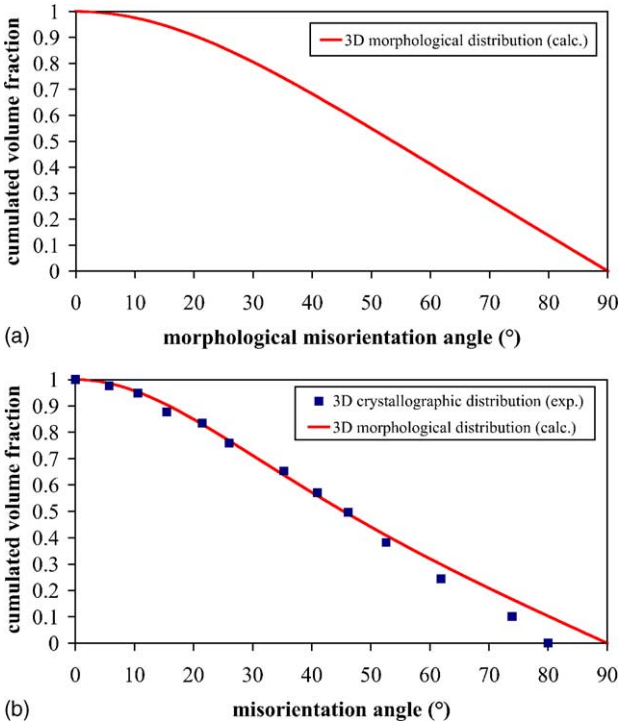

Fig. 13. Cumulated distribution of crystallographic misorientation angles (EBSD measurements) and morphological misorientation angles (from 2D image analyses): (a) non-oriented sample sintered at 1250 °C, (b) non-oriented sample sintered at 1300 °C.

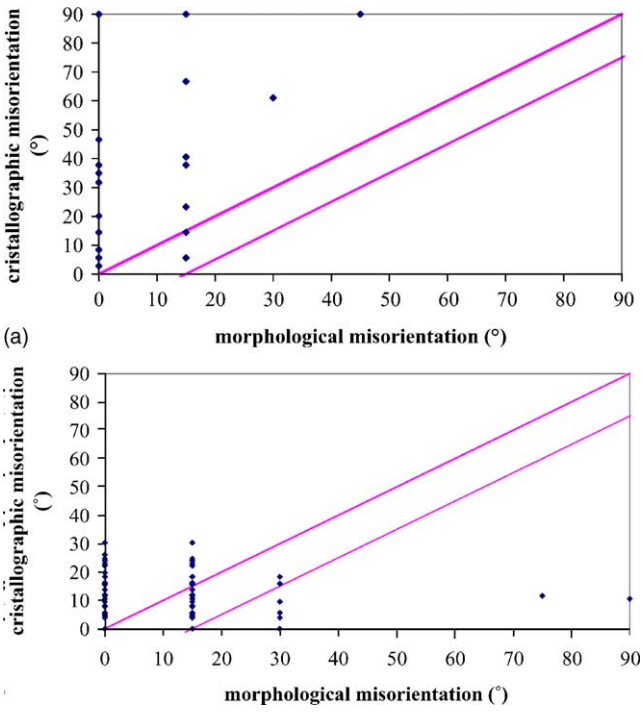

Fig. 14. Correlation between the crystallographic misorientation angle ω_C and the 2D morphological misorientation angle θ_M (the thick line represents the limit for $\theta_M \leq \omega_C$; the thin line is the limit for $\theta_M + 15^\circ \leq \omega_C$): (a) oriented sample sintered at 1250 °C, (b) oriented sample sintered at 1300 °C.

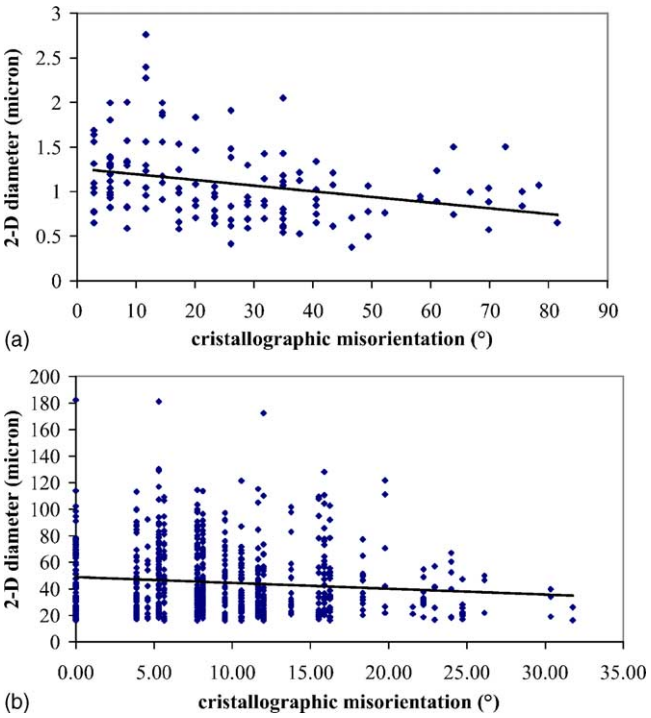

Fig. 15. Correlation between the 2D equivalent diameter and the crystallographic misorientation angle: (a) oriented sample sintered at 1250 °C, (b) oriented sample sintered at 1300 °C.

to morphological parameters (size, morphological orientation, ...). The major difficulty is that the local morphological measurements are 2D and correlation with 3D parameters needs a statistical treatment.

Let us assume that there is a perfect correlation between morphology and crystallography, i.e. plate-like grains have their large facets perpendicular to the [0 0 0 1] axis. Hence, for grains having their [0 0 0 1] axis at angle ω relative to the anisotropy axis, the normal to the large facet should form a dihedral angle ω relative to the anisotropy axis. From arguments developed above, the elongated 2D sections of these grains in a section containing the anisotropy axis should have a morphological misorientation angle θ comprised between 0 and ω. Fig. 14 plots the crystallographic misorientation angle ω_C *versus* the 2D morphological misorientation angle θ_M for elongated grains on the 2D images (only grains with shape factors $\geq$2 have been selected). A majority of points lies above the $\{\theta_M = \omega_C\}$ limit, taking into account the imprecision of 15° in the measurement of orientation angles in image analysis, showing that the morphological orientation of the grains is directly related to the crystallographic orientation, and then the morphological texture to the crystallographic texture.

Correlation of the crystallographic texture with grain size was also analysed. Fig. 15 plots the 2D diameter versus the crystallographic misorientation angle for all grains analysed in oriented samples sintered at 1250 and 1300 °C. There is a slight correlation between the 2D grain size and the crystallographic orientation: the largest particles seem to be better oriented in average. This correlation is probably sharper in 3D, since the 2D analysis can partly obliterate the trend: if large grains tend to be better oriented, small sections and large sections of these grains will appear as well oriented on the 2D images.

4. Discussion

The present results show the development of a morphological texture during the sintering of strontium hexaferrites, in relation with the crystallographic texture in the green body: grains tend to develop a plate-like shape and to align with their larger facets perpendicular to the anisotropy axis, i.e. the preferential orientation axis for the [0 0 0 1] crystallographic axis.

The role of sintering on the development of such a morphological texture will be discussed in a future paper but the main contribution is probably due to anisotropic grain growth. Indeed (0 0 0 1) facets usually have lower interfacial energies and lower mobilities in hexagonal structures and tend to grow laterally at the expense of other facets.[25] In oriented samples, those facets are initially preferentially perpendicular to the anisotropy axis, due to the high magnetocrystalline anisotropy field, and grain growth will then induce the development of plate-like grains which align preferentially with their larger facets perpendicular to the anisotropy axis. Since this morphological texture may

develop even for initially equiaxed grains, the fraction of aligned platelets will increase with grain growth, which explains the large texture enhancement between 1250 and 1300 °C (Table 2, Figs. 9 and 12). In non-oriented samples, the slight texture may be due to an initial morphological texture in the green body. Indeed, if plate-like grains are present in the powder, such grains would tend to align with their larger facets perpendicular to the anisotropy axis under the action of pressure. Even if grain growth is anisotropic, it does not produce a preferential orientation of platelets, excepted for initially aligned platelets: the morphological and crystallographic texture are then very similar, they are essentially controlled by the powder process and they hardly evolve with temperature (Table 2, Fig. 13). The higher 2D shape factor of the grains in oriented samples than in non-oriented samples is probably not an effect of a higher anisotropic grain growth but rather of a higher texture: sections in a plane containing the *Z*-axis will produce higher shape factors for plate-like grains if these grains align preferentially perpendicular to *Z* than if they are randomly oriented.

Finally, the crystallographic texture is observed to increase with temperature. This may be a consequence of grain growth. Indeed, small grains are on average not so well oriented (Fig. 15), probably because the moment exerted by the applied field during filter-pressing is smaller on these grains than on large grains. Grain growth increases the cristallographic texture, by eliminating the population of small badly oriented grains. As for material properties, grain growth is then beneficial for the saturation moment, but a too large contribution of grain growth, in particular abnormal grain growth, might decrease the coercivity[1].

5. Conclusion

Quantitative analysis of grain size, grain shape, morphological and crystallographic texture has been performed in strontium hexaferrite materials, sintered from filter-pressed powders oriented or not with a magnetic field. The results provide evidence for anisotropic and abnormal grain growth at high temperature ($T \geq 1250\,^{\circ}C$). A morphological texture develops during heating for oriented samples, with plate-like grains preferentially aligned with their larger facets perpendicular to the direction of field application. A quantitative analysis of the morphological texture in 3D has been performed and the relation between morphological and crystallographic texture could be analysed from the results. In non-oriented samples, the slight crystallographic texture is controlled by the initial morphological texture induced by compaction and both textures do not vary during sintering. In oriented samples, the initial crystallographic texture is responsible for the development of the morphological texture through anisotropic grain growth and both textures become similar at 1300 °C. Grain growth, by eliminating the population of small badly oriented grains, also explains the enhancement of the crystallographic texture. The influence of sintering on the texture will be discussed in a future paper.

Acknowledgements

The authors wish to thank Carbone-Lorraine/Ferrites and especially P. Tenaud for support, technical assistance and for fruitful scientific discussions.

References

1. Ataie, A., Harris, I. R. and Ponton, C. B., Magnetic properties of hydrothermally synthesized strontium hexaferrite as a function of synthesis conditions. *J. Mater. Sci.* 1995, **30**(6), 1429–1433.
2. Morisako, A., Saitoh, M. and Matsumoto, M., Magnetic properties of sputtered strontium ferrite films prepared from sintered target with Fe/Sr composition ratio of 8–14. *J. Appl. Phys.* 1999, **85**(8), 4732–4734.
3. Murillo, N., Gonzalez, J., Guraya, C., Gutierrez, M. and Seco, F. J., Structural and magnetic properties of sintered Sr-ferrites fabricated by powder injection molding. *J. Magn. Magn. Mater.* 1999, **203**(1–3), 165–168.
4. Duran, C., Trolier McKinstry, S. and Messing, G. L., Fabrication and electrical properties of textured $Sr_{0.53}Ba_{0.47}Nb_2O_6$ ceramics by templated grain growth. *J. Am. Ceram. Soc.* 2000, **83**(9), 2203–2213.
5. Ma, Y. and Wang, Z., To enhance Jc of Bi-2223 Ag-sheathed superconducting tapes by improving grain alignment with magnetic field. *Physica C* 1997, **282**(287), 2619–2620.
6. Pollert, E., Plechacek, V., Hejtmanek, J., Hudakova, N. and Chval, J., Optimization of the Bi(Pb)-2223 bulk technology. *Physica C* 1997, **282**(287), 2585–2586.
7. Tampieri, A., Celotti, G., Calestani, G. and Lesca, S., New technology to improve texturing and transport current in bulk (2223) BSCCO superconductors. *Key Eng. Mater.* 1997, **132–136**, 1247–1250.
8. Yanwei, M. and Zutang, W., To enhance critical current density of Ag-sheathed Bi(2223) superconducting tapes by a vibration technique. *Mater. Lett.* 1998, **34**(1/2), 95–98.
9. Hall, P. W., Swinnea, J. S. and Kovar, D., Fracture resistance of highly textured alumina. *J. Am. Ceram. Soc.* 2001, **84**(7), 1514–1520.
10. Li, C. S., Xi, Z. P., Zhang, P. X., Wu, X. Z. and Zhou, L., Fabrication of cold-rolled Ag-sheathed Bi(2223) tapes by a partial-melting process. *Physica C* 1997, **282**(287), 2611–2612.
11. Lu, C. H. and Chen, Y. C., Sintering and decomposition of ferroelectric layered perovskites: strontium bismuth tantalate ceramics. *J. Eur. Ceram. Soc.* 1999, **19**(16), 2909–2915.
12. Shui, A., Slaito, M., Uchida, N. and Uematsu, K., Development of anisotropic microstructure in uniaxially pressed alumina compacts. *J. Eur. Ceram. Soc.* 2002, **22**(8), 1217–1223.
13. Gruffel, P., Righetti, F. and Carry, C., Evolution of grain shape and size during high temperature creep of a yttria-doped fine-grained alumina. *J. Mater. Sci.* 1993, **28**, 2061–2066.
14. Xie, R. J., Mitomo, M., Kim, W. and Kim, Y. W., Texture development in silicon nitride–silicon oxynitride in situ composites via superplastic deformation. *J. Am. Ceram. Soc.* 2000, **83**(12), 3147–3152.
15. Yoshizawa, Y., Toriyama, M. and Kanzaki, S., Fabrication of textured alumina by high-temperature deformation. *J. Am. Ceram. Soc.* 2001, **84**(6), 1392–1394.
16. Seabaugh, M. M., Kerscht, I. H. and Messing, G. L., Texture development by templated grain growth in liquid-phase-sintered alpha -alumina. *J. Am. Ceram. Soc.* 1997, **80**(5), 1181–1188.
17. Horn, J. A., Zhang, S. C., Selvaraj, U., Messing, G. L. and Trolier McKinstry, S., Templated grain growth of textured bismuth titanate. *J. Am. Ceram. Soc.* 1999, **82**(4), 921–926.

18. Seabaugh, M. M., Messing, G. L. and Vaudin, M. D., Texture development and microstructure evolution in liquid-phase-sintered alpha-alumina ceramics prepared by templated grain growth. *J. Am. Ceram. Soc.* 2000, **83**(12), 3109–3116.
19. Suvaci, E. and Messing, G. L., Critical factors in the template grain growth of textured reaction-bonded alumina. *J. Am. Ceram. Soc.* 2000, **83**(8), 2041–2048.
20. Kools, F., Factors governing the alignment of sintered anisotropic M-type ferrites. *Berichte der Deutschen Keramischen Gesellschaft* 1978, **55**(6), 296–297.
21. Assis, O. B. G. and Ferrante, M., Magnetic texture enhancement densification, and grain growth in Nd–Fe–B permanent magnets. *J. Mater. Synth. Process.* 1995, **3**(2), 93–103.
22. Seabaugh, M. M., Vaudin, M. D., Cline, J. P. and Messing, G. L., Comparison of texture analysis techniques for highly oriented alpha-Al2O3. *J. Am. Ceram. Soc.* 2000, **83**(8), 2049–2054.
23. Kools, F., Morel, A., Grossinger, R., Le Breton, J. M. and Tenaud, P., LaCo-substituted ferrite magnets. *J. Magn. Magn. Mater.* 2002, **2**, 1270–1276.
24. Sandlin, M. S., Peterson, C. R. and Bowman, K. J., Texture measurement on materials containing platelets using stereology. *J. Am. Ceram. Soc.* 1994, **77**(8), 2127–2131.
25. Powers, J. D. and Glaeser, A. M., Grain boundary migration in ceramics. *Interf. Sci.* 1998, **6**(1/2), 23–39.